Tang T. & Huang L. (2022). Soundiation: A software in evaluation of acoustophoresis driven by radiation force and torque on axisymmetric objects. *The Journal of the Acoustical Society of America*.
DOI: 10.1121/10.0015199

Soundiation: A software in evaluation of acoustophoresis driven by radiation force and torque on axisymmetric objects

Tianquan Tang[1,2,*], Lixi Huang[1,2]

[1]*Department of Mechanical Engineering, The University of Hong Kong, Pokfulam, Hong Kong SAR, China*
[2]*Lab for Aerodynamics and Acoustics, HKU Zhejiang Institute of Research and Innovation, 1623 Dayuan Road, Lin An District, Hangzhou, China*

* Corresponding email: tianquan@connect.hku.hk

Acoustic radiation force and torque arising from wave scattering are commonly used to manipulate micro-objects without contact. We applied the partial wave expansion series and the conformal transformation approach to estimate the acoustic radiation force and torque exerted on the axisymmetric particles. Meanwhile, the translational and rotational transformations are employed to perform the prediction of the acoustophoresis. Although these theoretical derivations are well-developed [Tang and Huang, J. Sound Vibr. 532, 117012 (2022), Tang and Huang, Phys. Rev. E 105, 055110 (2022)], coding the required systems, including generation of the wave function, implementation of the transformations, calculations between modules, etc., is non-trivial and time-consuming. Here, we present a new open-source, MATLAB-based software, called Soundiation [GitHub Repository: https://github.com/Tountain/SoundiationAcoustophoresis, GPL-3.0 license], to address the acoustic radiation force and torque while supporting the dynamic prediction of non-spherical particles. The implementation is basically generic, and its applicability is demonstrated through the validation of numerical methods. A graphical user interface

(GUI) is provided so that it can be used and extended easily.

Keywords: Acoustic radiation force, Acoustic radiation torque, Acoustophoresis, Conformal mapping approach, GUI-based software.

I. Introduction

Acoustic tweezers use acoustic radiation force and torque to manipulate matter without contamination. The radiation force and torque are exerted on objects because of momentum and angular momentum transfers, respectively, that result from acoustic scattering and absorbing effects of the wave-particle interaction [1][2][3][4][5][6][7][8][9]. Since they are able to perform biocompatible, contact-free, and precise translation and rotation of micro-objects, this software greatly facilitates studies in engineering and biotechnology, including holographic acoustic tweezer [10][11][12], drug delivery [13], microorganism morphological interrogation [14], and microsurgery [15].

For Rayleigh objects, the Gor'kov theory is commonly employed to obtain the radiation force on the objects where the monopole and dipole scattering dominate [16]. Beyond the Rayleigh regime, the higher order scattering contributions become considerable and partially limit the application of Gor'kov theory. The radiation force and torque can be solved with the help of partial wave expansion series to account for the higher-order scattering contributions [17][18][19][20]. The above methods assume that the particles being manipulated are small or simple geometries. In reality, geometric asymmetry naturally exists in objects, such as *erythrocytes* [21] and *C. elegans* [24]. An alternative to evaluate the radiation force and torque on the non-spherical particles is the use of *T*-matrix [22][23] and numerical methods [21][25], while they may require relatively high computational cost and time-consuming.

To expand the range of applications while improving the efficiency in computations, in our previous studies, we established a general analytical framework to estimate radiation force and torque on any axisymmetric particles induced by traveling plane waves and user-customized transducer arrays [1][2][26]. We noted that a recent work presents a Python library to evaluate the radiation force on a single, spherical particle

in an infinite 3D-domain subjected to an incident plane standing or plane traveling wave [27], and the MATLAB codes used to evaluate the acoustic radiation force on spherical cells by a single-beam is given in [12]. Differently and generally, in this contribution, we present a high-performance and user-friendly graphical user interface (GUI), Soundiation, for the radiation force and torque, thereby the acoustophoretic process of the non-spherical objects. It is worth mentioned that the major theories applied in this software include partial wave expansion method [28], translation addition theorem [29], and conformal mapping approach [30]. The software is general in terms of particle geometries, particle sizes, and frequency range. Additionally, the user is able to decide the arrangement of the transducer configurations. The host fluid and particle boundary conditions also remain flexible. Some potential functionalities of this software are concluded as: (1) designing the non-spherical particle and generating its three-dimensional geometric data, which can be conveniently imported to other commercial numerical software (e.g., COMSOL Multiphysics) for further research; (2) visualizing the specified plane wavefield or piston-like wavefield from a user-customized transducer array; (3) estimating the acoustic radiation force and torque exerted on the particle designed in (1), and the incident wavefield is specified in (2); (4) predicting and visualizing the time-variant dynamic process of the particle designed in (1) under the incident wavefield given in (2), i.e., illustrating the time-variant acoustophoretic process of the particle.

The theoretical background and a brief overview of the software, Soundiation, is described in section 2 (more explanations on how to use the software can refer to the user manual given in the "SoundiationAcoustophoresis ./docs/user_manual" folder). In section 3, a series of radiation force and torque under different scenarios have been estimated and validated by the three-dimensional numerical simulations (the numerical model used to validate is given in the "SoundiationAcoustophoresis ./docs/COMSOL") folder, making the results acceptable in other applications. Additionally, we demonstrate an example, the

acoustophoretic process of an ellipsoid particle above a transducer array, to illustrate the ability of the software in prediction of dynamic processes. Finally, the impact and conclusions are described in sections 4 and 5, respectively.

II. Software description

A. Theoretical background

The reader is recommended to refer to our previous studies for more theoretical details in the determinization of mapping coefficients c_n [defined in Eq. (9) later] for different geometries [1], the coordinate transformation [2], the translation addition theorem in the transducer array system [26], and the radiation force and torque for the acoustophoretic process of particles [2]. Here, we only present the main formulas used in the software.

Firstly, we consider a time-harmonic acoustic plane wave with arbitrary incidence interacting with an axisymmetric body. The plane wave with wavenumber k can be formulated by a partial wave series as

$$\hat{\phi}_{\text{ex}} = \sum_{n,m} \bar{a}_{nm} J_n^m, \tag{1}$$

where the hat symbol $\hat{\cdot}$ represents the complex amplitude of the corresponding variable. Abbreviation $\sum_{n,m} \equiv \sum_{n=0}^{\infty} \sum_{m=-n}^{+n}$. Abbreviation variable J_n^m defines as a function $J_n^m(k\vec{r}) \equiv j_n(kr) Y_n^m(\theta, \phi)$ with $\vec{r} = (r, \theta, \phi)$. $j_n(kr)$ is the spherical Bessel function of order n at a position r, and $Y_n^m(\theta, \phi)$ is the spherical harmonic function of n-th order and m-th degree at the angular position (θ, ϕ). The beam-shape coefficients of the plane wave are [28]:

$$\bar{a}_{nm} = \mathrm{i}^n 4\pi Y_n^m(\theta_{\text{inc}}, \phi_{\text{inc}})^*, \tag{2}$$

where $Y_n^m(\theta_{\text{inc}}, \phi_{\text{inc}})$ is the spherical harmonic function of n-th order and m-th degree determined by the incidence angle of the incident plane wave $(\theta_{\text{inc}}, \phi_{\text{inc}})$. The asterisk symbol * means taking conjugation of the corresponding variable.

On the other hand, we consider the time-harmonic acoustic waves generated by an ultrasound transducer array (with the amplitude and phase parameters: A_i and α_i for the i-th transducer) interact with an axisymmetric particle. The total velocity potential amplitude from a whole transducer array can be obtained by a summation of the contributions from all transducers [26]:

$$\hat{\phi}_{\text{ex}} = \sum_{i=1}^{N_{\text{t}}} \hat{\phi}_{\text{trans}}^{(i)} = \sum_{n,m} [a]_{nm} J_n^m, \tag{3}$$

where the equivalent beam-shape coefficients

$$[a]_{nm} = \sum_{i=1}^{N_{\text{t}}} A_i \mathrm{e}^{\mathrm{i}\cdot\alpha_i} a_{nm}^{(i)}, \tag{4}$$

where $a_{nm}^{(i)} = \sum_{\nu,\mu} a_{\nu\mu} S_{\nu,n}^{\mu,m(1)}\left(k\vec{r}^{(iq)}\right)$, defined as the translation beam-shape coefficients of the i-th transducer. $S_{\nu,n}^{\mu,m(1)}\left(k\vec{r}^{(iq)}\right)$ is the separation transform matrix of the first kind [26]. Note that if $i = q$, $a_{nm}^{(q)} = \sum_{\nu,\mu} a_{\nu\mu} S_{\nu,n}^{\mu,m(1)}(0) = a_{nm}$. The beam-shape coefficients a_{nm} are numerically evaluated through the orthogonality properties of the spherical harmonics:

$$a_{nm} = \frac{1}{j_n(k\mathrm{R})} \int_0^{2\pi} \int_0^{\pi} \hat{\phi}_{\text{trans}}\left(\vec{\mathrm{R}}\right) Y_n^m(\theta,\phi)^* \sin\theta \, \mathrm{d}\theta \mathrm{d}\phi,$$

where $\vec{\mathrm{R}} = (\mathrm{R}, \theta, \phi)$ specifies a spherical space with a radius of R that contains the scatterer, not the sound sources. $\hat{\phi}_{\text{trans}}\left(\vec{\mathrm{R}}\right)$ is the potential field of the transducers at the surface $\vec{\mathrm{R}}$. Here, $\hat{\phi}_{\text{trans}}\left(\vec{\mathrm{R}}\right)$ is regarded as a circular piston-like radiator (refer to Eq. (4) in our previous work [2]). Note that term $j_n(k\mathrm{R})$ is possible to be zero in the calculations, so we need to add an extra small value (or function 'eps') to the denominator when solving for beam-shape coefficients.

Correspondingly, the scattering potential amplitude in the far-field can be expressed in terms of a partial wave series as:

$$\hat{\phi}_{\text{sc}} = \sum_{n,m} s_{nm} \tilde{a}_{nm} H_n^m, \tag{5}$$

where s_{nm} are the scalar scattering coefficients. Function $H_n^m \equiv H_n^m(k\vec{r}) \equiv h_n(kr) Y_n^m(\theta,\phi)$. $h_n(kr)$ is the spherical Hankel function of order n at a position r. $\tilde{a}_{nm} = \bar{a}_{nm}$ for the plane wave, while $\tilde{a}_{nm} = [a]_{nm}$ for the incident waves from a transducer array. For the sound-soft and sound-hard boundary conditions, the scalar scattering coefficients are obtained, respectively, by solving the following equations [1]

$$\sum_{n=0}^{\infty} \tilde{a}_{nm'} \Gamma_n^{n',m'} + \sum_{n=0}^{\infty} s_{nm'} \tilde{a}_{nm'} \Lambda_n^{n',m'} = 0, \quad (n' = 0,1,\cdots,\infty; m' = -\infty,\cdots,0,\cdots,\infty) \tag{6}$$

and

$$\sum_{n=0}^{\infty} \tilde{a}_{nm'} \Gamma_{n,u}^{n',m'} + \sum_{n=0}^{\infty} s_{nm'} \tilde{a}_{nm'} \Lambda_{n,u}^{n',m'} = 0. \quad (n' = 0,1,\cdots,\infty; m' = -\infty,\cdots,0,\cdots,\infty) \tag{7}$$

Here, the structural functions, $\Gamma_n^{n',m'}$ and $\Lambda_n^{n',m'}$, and their partial derivatives $\Gamma_{n,u}^{n',m'}$ and $\Lambda_{n,u}^{n',m'}$, are

$$\begin{cases} \Gamma_n^{n',m'} = \int_0^{\pi} j_n(kr) Q_n^m P_n^{m'}(\cos\theta) P_{n'}^{m'}(\cos w) \sin w \, \mathrm{d}w \Big|_{u=u_0} \\ \Lambda_n^{n',m'} = \int_0^{\pi} h_n(kr) Q_n^m P_n^{m'}(\cos\theta) P_{n'}^{m'}(\cos w) \sin w \, \mathrm{d}w \Big|_{u=u_0} \\ \Gamma_{n,u}^{n',m'} = \dfrac{\partial \Gamma_n^{n',m'}}{\partial u}\Big|_{u=u_0} \\ \Lambda_{n,u}^{n',m'} = \dfrac{\partial \Lambda_n^{n',m'}}{\partial u}\Big|_{u=u_0} \end{cases} \tag{8}$$

where $P_{n'}^{m'}(\cdot)$ represents the associated Legendre function of n'-th order and m'-th degree for the variable therein, and $Q_n^m = \sqrt{\frac{(2n+1)}{4\pi} \cdot \frac{(n-m)!}{(n+m)!}}$. Additionally, we provide a computational algorithm for the compressible non-spherical objects in Appendix II. The scalar scattering coefficients, s_{nm}, can be solved by Eq. (B.6) for the compressible (or Cauchy) boundary condition. By inserting the solved scalar scattering coefficients into Eqs. (10) and (11), we can evaluate the radiation force and torque, thereby the acoustophoresis of the compressible non-spherical objects.

In evaluation of the structure functions in Eq. (8), we need to provide the mapping relationship between the physical space and the mapping space. Specifically, the physical coordinates r and θ are connected with the mapping coordinates u and w by

$$\begin{cases} r(u,w) = \sqrt{f(u,w)^2 + g(u,w)^2} \\ \theta(u,w) = \cos^{-1}\big(g(u,w)/r(u,w)\big) \end{cases}, \tag{9a}$$

with the mapping functions $g(u,w)$ and $f(u,w)$ as

$$\begin{cases} g(u,w) = c_{-1}\mathrm{e}^{u}\cos(w) + \sum_{n=0}^{\infty} c_n \mathrm{e}^{-nu}\cos(nw) \\ f(u,w) = c_{-1}\mathrm{e}^{u}\sin(w) - \sum_{n=0}^{\infty} c_n \mathrm{e}^{-nu}\sin(nw) \end{cases}, \tag{9b}$$

where the mapping coefficients c_n are used to map the physical coordinate system to the mapping (spherical) coordinate systems. Finally, by inserting the mapping coefficients c_n, the structural functions ($\Gamma_n^{n',m'}$, $\Lambda_n^{n',m'}$, $\Gamma_{n,u}^{n',m'}$, $\Lambda_{n,u}^{n',m'}$), and the beam-shape coefficients ($\tilde{a}_{nm}$) into matrices (6) and (7), the unknown scalar scattering expansion coefficients (s_{nm}) of the non-spherical particle are determined. Note that the mapping coefficients c_n are different for various geometries [1][2][30], which should be acquired in advance and entered into the software.

Then, the acoustic radiation force and torque due to the incident and scattered fields on a particle are [1][2]

$$\begin{aligned} F_{\mathrm{rad},x} = +\frac{\rho_0}{4}\mathrm{Re}\Bigg[\mathrm{i} & \cdot \sum_{n,m} \tilde{a}_{nm}(1 + s_{nm})\big(\mathcal{A}_{n+1}^{m+1} b_{n+1,m+1}^{*} - \mathcal{B}_{n-1}^{m+1} b_{n-1,m+1}^{*} + \mathcal{C}_{n+1}^{m-1} b_{n+1,m-1}^{*} \\ & - \mathcal{D}_{n-1}^{m-1} b_{n-1,m-1}^{*}\big)\Bigg], \end{aligned} \tag{10}$$

$$\begin{aligned} F_{\mathrm{rad},y} = +\frac{\rho_0}{4}\mathrm{Re}\Bigg[\sum_{n,m} \tilde{a}_{nm}(1 & + s_{nm})\big(\mathcal{A}_{n+1}^{m+1} b_{n+1,m+1}^{*} - \mathcal{B}_{n-1}^{m+1} b_{n-1,m+1}^{*} - \mathcal{C}_{n+1}^{m-1} b_{n+1,m-1}^{*} \\ & + \mathcal{D}_{n-1}^{m-1} b_{n-1,m-1}^{*}\big)\Bigg], \end{aligned}$$

$$F_{\mathrm{rad},z} = +\frac{\rho_0}{2}\mathrm{Re}\left[\mathrm{i}\cdot\sum_{n,m}\tilde{a}_{nm}(1+s_{nm})\left(\mathcal{E}_{n+1}^{m}b_{n+1,m}^{*}-\mathcal{F}_{n-1}^{m}b_{n-1,m}^{*}\right)\right],$$

and

$$T_{\mathrm{rad},x} = +\frac{\rho_0}{4k}\mathrm{Re}\left[\sum_{n,m}\tilde{a}_{nm}(1+s_{nm})\left(\mathcal{G}_{n}^{m}b_{n,m+1}^{*}+\mathcal{G}_{n}^{-m}b_{n,m-1}^{*}\right)\right], \tag{11}$$

$$T_{\mathrm{rad},y} = -\frac{\rho_0}{4k}\mathrm{Re}\left[\mathrm{i}\cdot\sum_{n,m}\tilde{a}_{nm}(1+s_{nm})\left(\mathcal{G}_{n}^{m}b_{n,m+1}^{*}-\mathcal{G}_{n}^{-m}b_{n,m-1}^{*}\right)\right],$$

$$T_{\mathrm{rad},z} = +\frac{\rho_0}{2k}\mathrm{Re}\left[\sum_{n,m}\tilde{a}_{nm}(1+s_{nm})mb_{n,m}^{*}\right],$$

where ρ_0 is the density of the host fluid, abbreviation $b_{nm} = \tilde{a}_{nm}\cdot s_{nm}$, and symbol Re means taking the real part of the expression. The weighting coefficients $\mathcal{A}_n^m = -\mathcal{C}_n^{-m} = -\sqrt{\frac{(n+m-1)(n+m)}{(2n-1)(2n+1)}}$, $\mathcal{B}_n^m = -\mathcal{D}_n^{-m} = \sqrt{\frac{(n-m+2)(n-m+1)}{(2n+1)(2n+3)}}$, $\mathcal{E}_n^m = \mathcal{F}_{n-1}^m = \sqrt{\frac{(n-m)(n+m)}{(2n-1)(2n+1)}}$, and $\mathcal{G}_n^m = \sqrt{(n-m)(n+m+1)}$. Note that we need to truncate the infinite summation $\sum_{n,m} \equiv \sum_{n=0}^{\infty}\sum_{m=-n}^{+n}$ to $\sum_{n,m} \equiv \sum_{n=0}^{N}\sum_{m=-n}^{+n}$ using a truncation number $N \geq ka+6$ [31] so that we could perform the predictions of Eqs. (10) and (11). Another detail to note is that the terms $\tilde{a}_{n-1}^{m+1}$, $\tilde{a}_{n+1}^{m+1}$, $\tilde{a}_{n-1}^{m-1}$, $\tilde{a}_{n+1}^{m-1}$, $\tilde{a}_{n}^{m+1}$, and $\tilde{a}_{n}^{m-1}$ included in Eq. (10) and (11) do not always exist in physics. Taking $\tilde{a}_{n-1}^{m+1}$ as an example, when it comes to calculate $\sum_{n,m}\tilde{a}_{n-1}^{m+1} \equiv \sum_{n=0}^{N}\sum_{m=-n}^{+n}\tilde{a}_{n-1}^{m+1}$, if $m=n$, index $m+1 \to n+1 > n$, which means that for calculation of $\sum_{n=0}^{N}\sum_{m=-n}^{+n}\tilde{a}_{n-1}^{m+1}$, the physically meaningful range of m should satisfy $|m+1| \leq (n-1)$. The right regime of index m is also pointed out and explained in [17]. For other terms $\tilde{a}_{n+1}^{m+1}$, $\tilde{a}_{n-1}^{m-1}$, $\tilde{a}_{n+1}^{m-1}$, $\tilde{a}_{n}^{m+1}$, and $\tilde{a}_{n}^{m-1}$, similar constraints should be considered in the calculations. Only the physically meaningful elements involve in the calculations [The users can refer to lines 97 to 107, lines 131 to 141, lines 165 to 175, and lines 199 to 209 of code "radiation_force_based_Analyses.m" to check how to constrain the regimes of $\tilde{a}_{n+1}^{m+1}$, $\tilde{a}_{n-1}^{m+1}$, $\tilde{a}_{n+1}^{m-1}$, and $\tilde{a}_{n-1}^{m-1}$, respectively]. It is worth mentioned that the above derivations could be extended to the scenarios when the objects are suspended in the electromagnetic field [32].

The objects are driven by acoustic radiation force and torque, while partially impeded by the Stokes drag force and torque. Here, the drag force and torque can be

determined with the help of numerical methods for non-spherical particles [21], we try to avoid the numerical process delaying our dynamic calculations, and thus they are approximately evaluated using classical formulas [33][34]

$$\vec{F}_{\mathrm{drag}} = -6\pi a\eta\vec{u}_{\mathrm{p}}, \tag{12}$$

and

$$\vec{T}_{\mathrm{drag}} = -8\pi a^3\eta\vec{\omega}_{\mathrm{p}}, \tag{13}$$

where a is averaged radius of the particle and η is the dynamic viscosity of the host fluid. The particle velocity $\vec{u}_{\mathrm{p}}$ and particle angular velocity $\vec{\omega}_{\mathrm{p}}$ are based on the relative velocity of the particle with respect to the background fluid. Then, the dynamic process is described by the equation of motion as

$$m_{\mathrm{p}}\frac{\mathrm{d}\vec{u}_{\mathrm{p}}}{\mathrm{d}t} = \vec{F}_{\mathrm{rad}}+\vec{F}_{\mathrm{drag}}+\vec{F}_{\mathrm{G}}, \tag{14}$$

and

$$I_{\mathrm{p}}\frac{\mathrm{d}\vec{\omega}_{\mathrm{p}}}{\mathrm{d}t} = \vec{T}_{\mathrm{rad}}+\vec{T}_{\mathrm{drag}}. \tag{15}$$

where m_{p} is the mass of the particle and I_{p} is the moment of inertia of the particle. $\vec{F}_{\mathrm{G}}$ are the gravity of the particle. Through solving Eqs. (14) and (15), particle velocity and angular velocity can be obtained. As a result, the time-dependent trajectory is solved based on a simple time accumulation method by providing an initial state for the particle with a time step of Δt. The particle displacement and rotation angle using particle velocity and angular velocity in current time step through $\vec{r}_{\mathrm{t}} = \vec{r}_{\mathrm{t}} + \Delta\vec{r}_{\mathrm{t}}$ with $\Delta\vec{r}_{\mathrm{t}} = \vec{u}_{\mathrm{p}}\Delta t$, and $\vec{\theta}_{\mathrm{rot}} = \vec{\theta}_{\mathrm{rot}} + \Delta\vec{\theta}_{\mathrm{rot}}$ with $\Delta\vec{\theta}_{\mathrm{rot}} = \vec{\omega}_{\mathrm{p}}\Delta t$.

B. Software architecture

Here, a brief summary of the major features is presented below. For user-friendly considerations, the software is demonstrated as a GUI, which has been tested with MATLAB 2010a and above versions. The current code version and permanent link to code are given in Appendix I. When we run the GUI ("main_interface.m"), a set of

default parameters is given, while the users can change all the parameters based on their needs. The source codes can be found in the "SoundiationAcoustophoresis ./src" folder, while the explanation of parameters required in the graphical user interface (GUI) can be found in the "SoundiationAcoustophoresis ./docs/user_manual" folder. As shown in Fig. 1, the GUI of Soundiation is divided into three main panels, "Visualization", "Calculation controls", and "Functions".

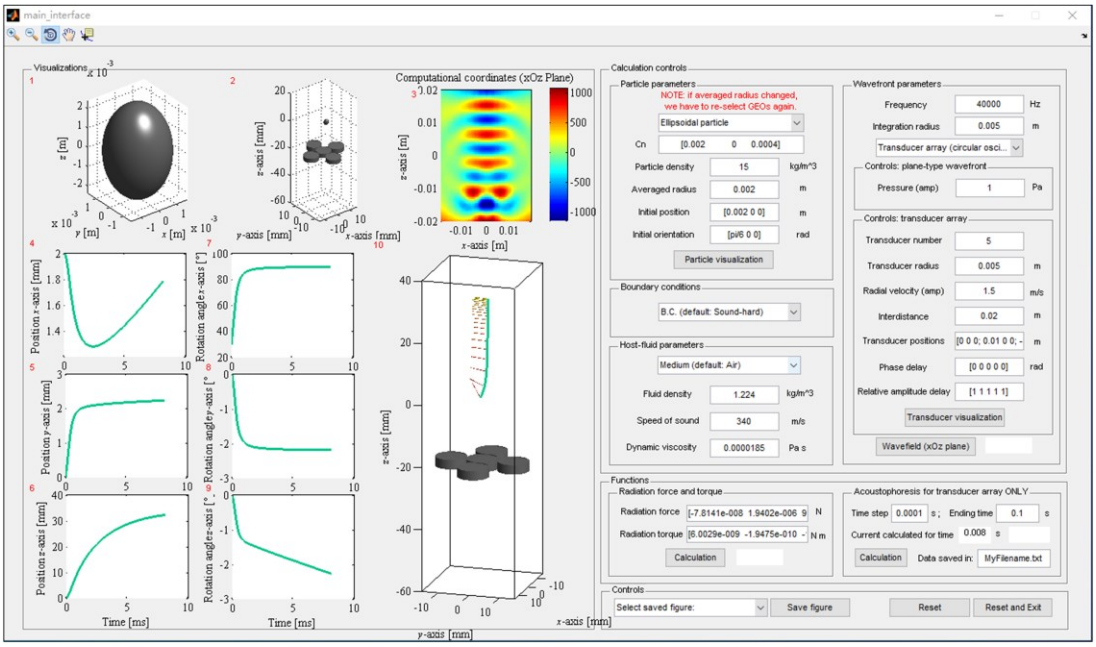

Figure 1: Graphical user interface (GUI) of Soundiation.

The first penal, "Visualization", is designed to visualize the optional results, including geometry of particle, transducer-particle system, incident wavefield, and time-variant trajectory of particle driven by the acoustic incident wavefields (i.e., acoustophoretic process). The "Visualization" panel has ten regions, labeled from 1 to 10. Note that all figures illustrated in the "Visualization" panel can be saved using the "Save figure" button.

The second panel, "Calculation controls", defines the computational conditions, geometric information, and material properties. Specifically, there are four kinds of controlling parameters. Firstly, the geometry and physical properties of a particle must

be defined. Secondly, the boundary condition to the particle surface should be selected, including the sound-hard (Neumann) and the sound-soft (Dirichlet) boundary conditions. Thirdly, the medium that immersed the particle should be selected. Finally, the incident wavefield should be specified by giving the complex pressure amplitude for the plane wavefront or the transducer parameters for the wavefront of the transducer array.

The final panel, "Functions", provides two optional calculations based on the parameters set in the "Calculation controls" panel. The first sub-panel provides functionality to directly predict the acoustic radiation force and torque exerting on the user-specified particle under user-customized incident wavefront. The second sub-panel is designed to compute a dynamic process for the scenario that any axisymmetric, irregular particle levitated above a user-customized transducer array. The time-variant trajectories, including translational and rotational information, are visualized in the "Visualization" panel.

C. Software functionalities

Soundiation is designed to efficiently estimate the radiation force and torque on various particles under a sound wavefield. Combined with the viscous drag force and torque [33][34], the spatio-temporal acoustophoresis of these particles can be predicted. It should be emphasized that the user can design the shape of particles, including spherical or arbitrary axisymmetric geometries. Furthermore, the incident wavefield also supports user-customized. These geometric degrees of freedom greatly improve the application of this software in a wider range of scenarios. More specifically, the functionalities and instructions are introduced in detail below.

1. Particle-transducer system and incident wavefield visualization

A three-dimensional graph of the manipulated non-spherical particle can be designed by specifying the mapping coefficients c_n [1]; the corresponding geometry

is illustrated in the "Visualization" panel (labeled by 1, Fig. 1). The surface coordinates are automatically saved in the "particle_data.stl" file, which facilitates the import of particle geometry into other numerical software (e.g., COMSOL Multiphysics) and generates three-dimensional structures to perform numerical calculations if needed. The geometric differences are captured by different combinations of the mapping coefficients c_n [1], while the general geometric size can be stretched by changing the parameter of "Averaged radius". It should be emphasized that the first coefficient of the mapping coefficients is equivalent to the averaged radius. After clicking the "Particle visualization" button, the particle geometry is plotted in the "Visualization" panel.

Additionally, for the case of using transducer arrays, three-dimensional visualization of the particle-transducer system is available. Note that to graph the result, the user needs first to initialize and parameterize the particle and the transducer array. Particle "Initial position" represents the values that the particle deviates from the coordinate origin $(0,0,0)$, while particle "Initial orientation" gives the angles that the particle rotates along the x-, y-, and z-axes, respectively. For example, if "Initial position = $[0.002,\ 0,\ 0]$ m" and "Initial orientation = $[\pi/6,\ 0,\ 0]$ rad", the particle should be placed at $x = 2$ mm, $y = 0, z = 0$ and be rotated along x-axis for $\pi/6$ rad. Similarly, all transducers should be parameterized. The number, radius, and positions of transducers should be specified in "Transducer radius", "Transducer number", and "Transducer positions". A $N \times 3$ matrix is required to define the position, where N corresponds to the number of transducers, and their central positions are recorded in the row vectors. The first transducer is defined as the probe transducer, whose Cartesian coordinates are set to $(0,0,0)$, while the coordinates of the other transducers are given relative to the probe transducer. As a result, any desirable distribution of transducers is possible. Note that the "Transducer positions" given above are under the premise that the probe transducer coincides with the coordinate origin. To change the vertical position of the transducer array, the parameter

"Interdistance" is introduced, which indicates a value that translates the array along $-z$-axis. After clicking the "Transducer visualization" button, the particle-transducer system is depicted in the "Visualization" panel (labeled by 2, Fig. 1).

Soundiation uses the partial wave expansion series to describe incident wave propagation in the invisous medium [28]. The method gives either a plane wavefield or a summation wavefield from multiple circular radiators (or transducers). It should be emphasized that the vibration of each circular radiator can be regarded as a piston-like vibrator whose wavefield is well-known [35], and thus the summation wavefield can be derived with the help of the translation addition theorem [2][26]. Before visualizing the incident wavefield, the user needs to first parameterize the wavefront parameters in the GUI. Apart from the "Frequency", the user is required to define the pressure amplitude in "Pressure (amp)" for the plane traveling wave, while the amplitude of radial velocity and the array delay (phase and relative amplitude delays) in "Radial velocity (amp)", "Phase delay", and "Relative amplitude delay". In this way, once the incident wavefront parameters have been specified, a pressure wavefield on xOz plane is available to give an impression of the incident wave patterns in "Visualization" panel (labeled by 3, Fig. 1) by clicking the "Wavefield (xOz plane)" button.

2. Acoustic radiation force and torque on non-spherical particles

This module calculates radiation force and torque exerted on the axisymmetric particles excited by a plane wave or a user-customized transducer array (see Eqs. (10) and (11)).

Parameter definitions of particles and incident wavefields are explained in section 2.3.1. In order to estimate the radiation force and torque, except to parameterize the particles and the incident wavefront, the user needs to specify the boundary condition (around the particle surface) and the medium properties. The medium properties can be simply defined by selecting an in-house medium from the popup menu in the "Host-

fluid parameters" sub-panel. Physically, the sound-soft (Dirichlet) and the sound-hard (Neumann) boundary conditions require that the total potential vanishes and the normal particle velocity vanishes, respectively, on the scatterer surface. A detailed derivation can be found in our previous work [1][2]. Nevertheless, from the user's point of view, there is no need to enter the detail of all the related formulas. The GUI provides a convenient way to build the boundary condition around the scatterer surface by selecting a desirable one from the popup menu in the "Boundary conditions" sub-panel.

After completing all the above settings, the corresponding radiation force and torque will be presented in the edit boxes "Radiation force" and "Radiation torque" by clicking the "Calculation" button in the "Radiation force and torque" sub-panel (the computation will take a few seconds). The data is given in the format of a 1×3 row vector, representing the radiation force and torque components in the x-, y-, and z-directions, respectively.

3. Dynamic process: particle acoustophoresis

The software is able to predict the spatio-temporal trajectories of a user-defined particle under the acoustic field, i.e., the acoustophoretic process (described by Eqs. (14) and (15)). Consider that the particle is driven by acoustic radiation force and torque, while delayed by the drag force and torque due to the viscous stresses and shear stresses on the particle surface [33][34]. Since the drag force and torque is proportional to the particle relative velocity and angular velocity, which source from the radiation force and torque. Therefore, the time-dependent process is obtainable. Once the initial status of the particle is given, the radiation force and torque can be evaluated. As a result, the particle velocity and angular velocity (i.e., the drag force and torque) can be solved following the equation of motions. Then, these velocities are applied to renew the particle position and orientation for the next time step [2].

To carry on the prediction of the acoustophoretic process, except for the settings

given in sections 2.3.1 and 2.3.2 for the radiation force and torque for the initial status, the user needs to specify further an ending moment ("Ending time") to stop the prediction and a time step ("Time step") to continue the computation. Note that we end the predictions when the positions and rotation angles change among two adjacent time steps are less than 5%. It should also be mentioned that the in-house wavefield radiated from a circular oscillator is based on the far-field assumption [35]. Therefore, we stop the calculations once the vertical distance (or interdistance) between the particle and the transducer array is smaller than 10 mm, which is close to a wavelength of the operating frequency in the air.

Prediction begins after clicking the "Calculation" button in the "Acoustophoresis for transducer array" sub-panel. And the predicted translational and rotational trajectories are depicted in the "Visualization" panel. The time-variant translational trajectories along x-, y-, and z-axes are plotted in the "Visualization" panel, labeled by 4, 5, and 6 (Fig. 1), respectively. The time-variant rotational tendencies along x-, y-, and z-axes are graphed in blank regions 7, 8, and 9 (Fig. 1), respectively. Correspondingly, a three-dimensional result is given in region 10 (Fig. 1), where the solid line indicates the translational trajectory while the arrows demonstrate the particle orientation (axisymmetric axis). The color of the arrow is used to represent the increase of time (red-yellow color spectrum). The time intervals represented by any adjacent arrows are the same. We apply a total of 20 arrows to continuously demonstrate the rotational property of the particle from the start of the calculation (red arrow) to the end of the calculation (yellow arrow). Additionally, the control parameters and the corresponding dynamic process (i.e., the translational positions and the rotational angles at different time steps) are recorded in a user-defined ".txt" file automatically. By default, the file name is "Myfilename.txt".

III. Illustrative Results

Here, we predict the radiation force and torque (see Eqs. (10) and (11)) on different particles using the Soundiation software (GUI), followed by comprehensive validations with numerical results from COMSOL. A cubic region is defined as the simulation domain. The center of mass of the irregular object and the center of the simulation domain are both placed at the origin of the Cartesian coordinate system. A spherical surface is defined as the integration surface for the acoustic information to compute the numerical radiation force and torque. A detailed numerical scheme under the Cartesian coordinate system is given in Appendix D of [1]. The perfect matched layer (PML) is applied around the simulation domain to remove additional reflections of sound waves. The incident plane wave is simulated by giving a "background pressure field", while the sound radiation from the transducers is modeled by setting a "radial vibrated velocity" on the transducer surfaces. More details can be found in the COMSOL file downloaded in "SoundiationAcoustophoresis ./docs/COMSOL". Afterward, we demonstrate an example to predict the spatio-temporal acoustophoretic process of a non-spherical particle above a transducer array.

A. Validations: radiation force and torque on various particles

The particles can be created by specifying proper mapping coefficients and clicking the "Particle visualization" in the "Particle parameters" sub-panel, as shown in Fig. 1. The corresponding particle geometry will be present in region 1 of the "Visualization" panel; meanwhile, the geometric data is automatically saved in the "particle_data.stl" file. Then, the data file can be directly imported into COMSOL to establish the numerical model and, if required, validate the predictions.

For the first example, consider that a time-harmonic acoustic plane wave interacts with different axisymmetric particles (including cone and cylindrical particles with mapping coefficients of c_n = [0.002 0 0 0.00025] and c_n = [0.002 0 -0.0005 0 -

0.00025], respectively) at different particle orientations. The designed cone and cylindrical particles are illustrated in Figs. 2(a) and 3(a). We assume that the particles are all rigid, corresponding to the sound-hard or Neumann boundary condition, and their averaged radius is set to 2 mm. The plane wave is propagating in the air, operating at a frequency of 40 kHz and a pressure amplitude of 1 Pa. To demonstrate and validate the software property in predicting the radiation force and torque under a plane wavefield, we compare the predicted results and the numerical simulations as shown in Figs. 2 and 3. In all cases, the particle position is set to [0 0 0]. Differently, the particle orientation varies along x-axis, that is $\theta_{\mathrm{rot},x} \in [0, 90^{\circ}]$.

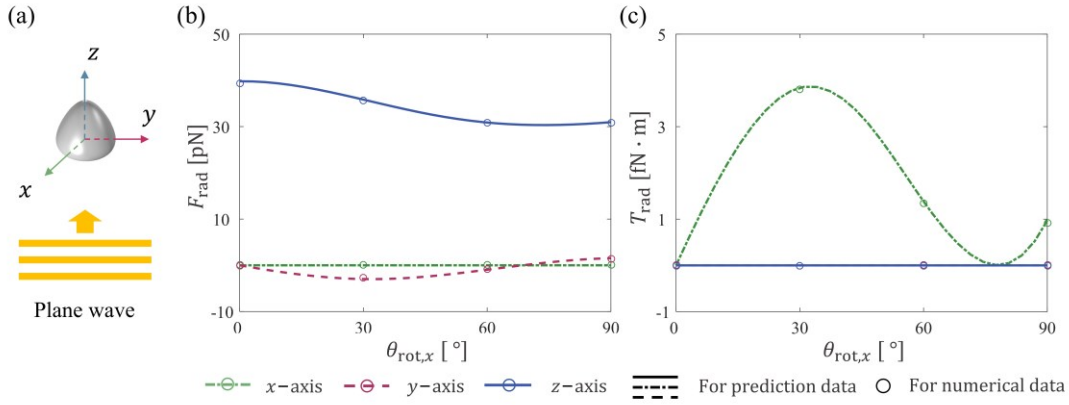

Figure 2: Theoretical and numerical calculations of the acoustic radiation force, $\vec{F}_{\mathrm{rad}}$, and torque, $\vec{T}_{\mathrm{rad}}$, resulting from an incident plane wave (amplitude of 1 Pa) acting on a sound-hard cone particle (averaged radius of 2 mm) as a function of the particle orientation $\theta_{\mathrm{rot},x} \in [0, 90^{\circ}]$. (a) Schematic diagram of a plane wave interacting with the cone particle under the Cartesian coordinate system. (b) and (c) Comparison plots for the radiation force and torque, respectively. The green dashed-dot lines, red dashed lines, and the blue solid lines indicate the prediction data along x-, y-, and z-axes, while the circle marks represent the corresponding results based on the full three-dimensional numerical simulations.

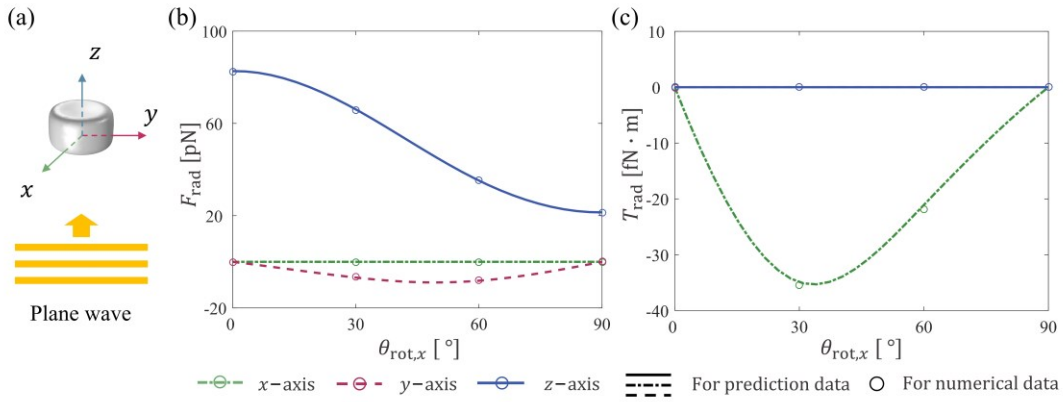

Figure 3: The same as in Fig. 2, but the scatterer is changed to a cylindrical particle.

For another example, we consider that a diamond particle (c_n = [0.002 0 0 0 0.0002]) is levitated above a transducer array. The particle is rigid (sound-hard or Neumann boundary condition), and its averaged radius is also set to 2 mm. The diamond particle used here is shown in Fig. 4(a) (or Fig. 5(a)). The sound waves radiated from the circular radiators, the amplitude of the radial velocity of 1.5 m/s, are propagating in the air, operating at a frequency of 40 kHz. The transducer array consists of four transducers with radii of 5 mm. The transducer configuration, phase delay, and relative amplitude delay are arranged as shown in Fig. 4(a) or 5(a). Specifically, we define "Transducer positions" as $[0\ 0\ 0;\ 0.01\ 0\ 0;\ -0.01\ 0\ 0;\ 0\ 0.01\ 0]$ m, "Phase delay" as $[0\ 0\ \pi/2\ 0]$ rad, and "Relative amplitude delay" as $[1\ 1\ 1\ 1]$. The predicted radiation force and torque are validated by the numerical method, as illustrated in Figs. 4 and 5. The interdistance is set to 20 mm to reduce the number of mesh elements in the full three-dimensional numerical model, which greatly saves simulation time. The particle is fixed in [0 0 0] position, while its orientation varies along x-axis or y-axis, i.e., $\theta_{\mathrm{rot},x} \in [0, 90^{\circ}]$ or $\theta_{\mathrm{rot},y} \in [0, 90^{\circ}]$.

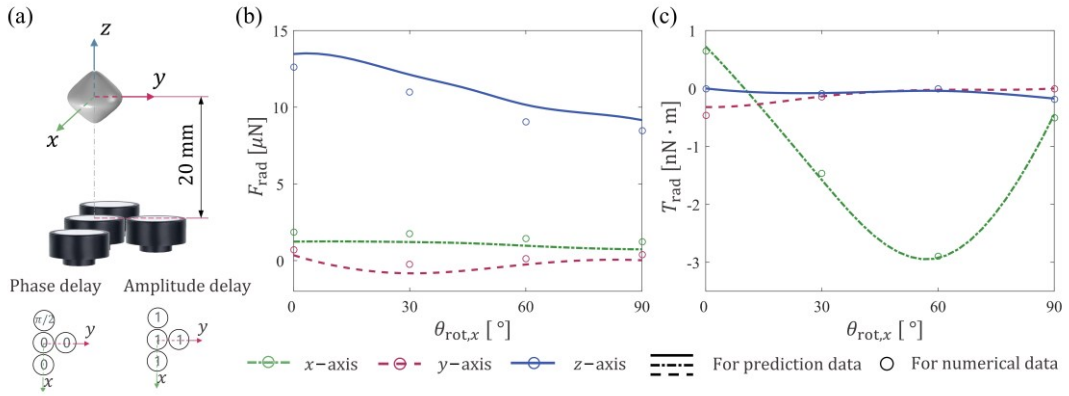

Figure 4: Theoretical and numerical calculations of the acoustic radiation force, $\vec{F}_{\mathrm{rad}}$, and torque, $\vec{T}_{\mathrm{rad}}$, acting on a sound-hard diamond particle (averaged radius of 2 mm) as a function of the particle orientation $\theta_{\mathrm{rot},x} \in [0, 90^{\circ}]$ in a four-transducer system. (a) Schematic diagram of the particle-transducer system and the phase and amplitude distributions of the transducer array. (b) and (c) Comparison plots for the radiation force and torque, respectively. The meanings of the circle marks and the curves are the same as those described in Fig. 2.

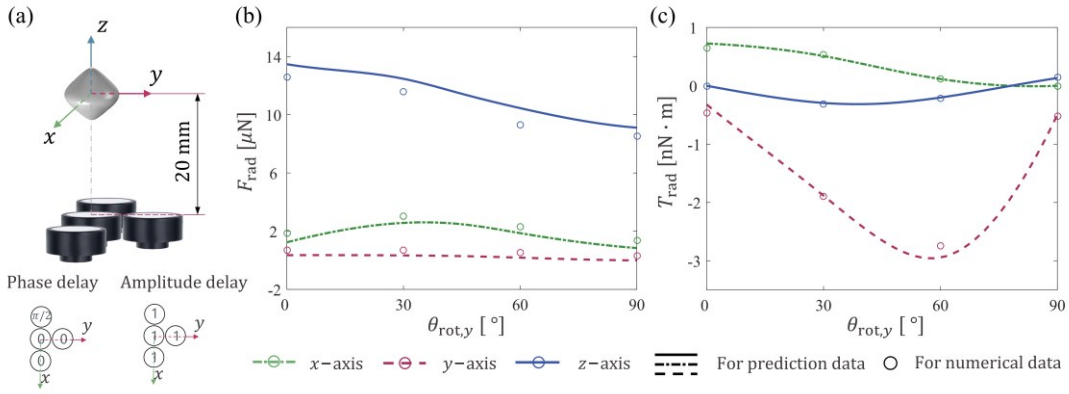

Figure 5: The same as in Fig. 4, but the particle orientation θ_{rot} is varied along y-axis.

It can be found in Figs. 2, 3, 4, and 5 that the acoustic radiation force and torque between our method and the numerical method are perfectly matched in various scenarios. However, it should be emphasized that for the cases using a transducer array, since the distance between the scatterers and the transducer array is relatively small (i.e., the interdistance is 20 mm), the wavefield around the scatterers does not meet the far-field requirements, which compromises the prediction accuracy shown in Figs. 4 and 5.

Furthermore, it is worth mentioned that Soundiation merely takes about ten seconds to estimate the radiation force and torque, while the numerical counterparts will cost about ten minutes (CPU: Intel i7-6700HQ 2.6 GHz; Maximum memory usage: 16 GB). Hence, the software becomes significant because it shows high computational accuracy and good computational robustness, while requiring much less computational time. Additionally, the validated COMSOL model, "Radiation_force_torque.mph", is accessible from the "SoundiationAcoustophoresis ./docs/COMSOL" folder.

B. Prediction of the acoustophoretic process

In this section, we illustrate another functionality in the prediction of the acoustophoresis of an ellipsoidal particle ($c_n = [0.002\ 0\ 0.0004]$) above a transducer array using Soundiation. The ellipsoidal particle is rigid (sound-hard or Neumann boundary condition) with a density of $\rho_\mathrm{p} = 15\ \mathrm{kg/m^3}$, and its averaged radius is also set to $a = 2\ \mathrm{mm}$. In this way, the gravity can be calculated by $F_\mathrm{G} \approx \frac{4}{3}\pi a^3 \rho_\mathrm{p} g$, where g is the acceleration of gravity. The ellipsoidal particle is shown in Fig. 6(a). The amplitude of the radial velocity of the transducers is also set to 1.5 m/s, with a vibration frequency of 40 kHz. The transducer array consists of five transducers with radii of 5 mm. The transducer configuration, phase delay, and relative amplitude delay can refer to Figs. 6(a) and 6(b). The initial particle position is given at [2 0 0] mm of Cartesian coordinates, while the particle rotates along x-axis for $\pi/6$, or $\theta_{\mathrm{rot},x} = \pi/6$, as the initial particle orientation. The interdistance is set to 20 mm. The ending time and the time step are set to 0.1 s and 0.0001 s, respectively.

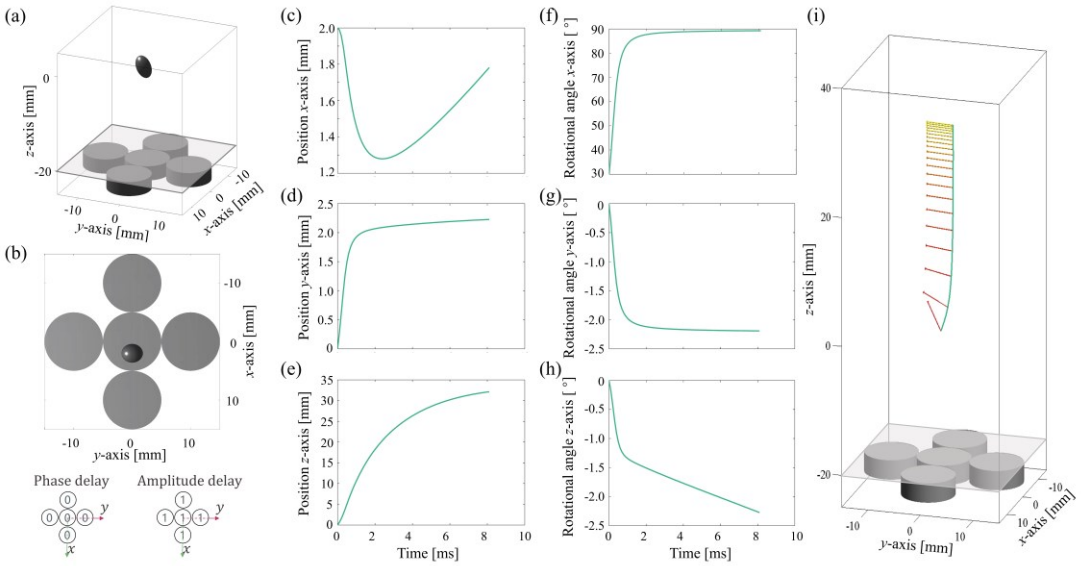

Figure 6: The time-variant translational and rotational trajectories of a sound-hard ellipsoidal particle with an averaged radius of 2 mm, manipulated by a transducer array. (a) The initial status of the particle-transducer system. The particle is placed at $(x, y, z) = [2, 0, 0]$ mm, rotating along x-axis with $\pi/6$. The interdistance is set to 20 mm. All transducers operate with the same phase and vibration amplitude. (b) The top view of the particle-transducer system (a). (c), (d), and (e) The translational trajectories of the particle along x-, y-, and z-axes, respectively. (f), (g), and (h) The rotational trajectories of the particle along x-, y-, and z -axes, respectively. (i) The time-variant translational trajectory (solid line) and particle orientation (arrow) visualized in three-dimensional. These arrows represent the axisymmetric axis of the particle, while the color of the arrow is used to represent the increase of time (red-yellow color spectrum). The time intervals represented by any adjacent arrows are the same. These are 20 arrows showing the position and orientation of the particles from the start of the calculation (red arrow, 0 s) to the end of the calculation (yellow arrow, 0.008 s).

Figure 6 shows that the time-variant translational and rotational trajectories of an ellipsoidal particle can predict using the software, indicating that it is able to apply in describing the motion of various objects with a step-by-step and user-friendly guide approach. The prediction ends at 0.008 s (before 0.1 s) since the error of the positions and the rotation angles among two adjacent time steps are less than 5%.

IV. Impact

Soundiation is a GUI-based software that allows users to design arbitrary axisymmetric geometries and evaluate the radiation force and torque exerted on them. Furthermore, the software supports user-customized incident wavefronts, including the transducer configurations and corresponding transducer parameters. Based on the derived radiation force and torque, taking into account the effects of viscosity, the dynamics of a non-spherical particle can be predicted and visualized. The above functionalities are beneficial for researchers who study axisymmetric micro- or nano-objects manipulation using the radiation force and torque in bioengineering [36][37] and medical [38][39] industries.

In addition to being suitable for a wider range of working parameters and application scenarios, Soundiation exhibits superior computational accuracy, high geometric adaptivity, and good robustness to various geometric features, while the computational efficiency is much higher than that of the full numerical methods. The time-consuming numerical simulations make the time-variant acoustophoretic process unpredictable, while this is possible in Soundiation since the computational time typically takes about ten seconds per time step in common personal computers. Moreover, the user-friendly GUI-based application facilitates effortless use of the software by researchers unfamiliar with the theoretical principles.

Furthermore, the open-source codes allow researchers to add their features under the current framework and test new algorithms for other projects. For example, while the software merely supports the plane wavefronts or the wavefronts of circular radiators (or transducer array) in the current version, it can be simply extended to user-dependent arbitrary wavefronts through defining the proper wave functions in the source code “wave_function.m”.

V. Conclusions

Soundiation is software that computes the radiation force and torque on user-specified axisymmetric particles under a user-customized incident wavefield (plane-wave mode or transducer-array mode). Geometric data for user-designed particles is automatically saved and can be imported directly into commercial numerical software (such as COMSOL Multiphysics) when needed to validate the predictions. It can be found that the predicted data are in perfect agreement with the direct numerical simulations, while the computational efficiency is much higher. Driven by radiation force and torque, the dynamics (or acoustophoresis) of any user-defined particle above the user-customized transducer array can be predicted and visualized. Additionally, the user-friendly GUI grants the users many advantages, making the software easier to use and extend, more efficient, and significantly reducing the learning curve for new users. The proposed software can be an effective tool to predict the motions of various non-spherical objects, helping to understand the acoustophoretic phenomena with a wide range of parameters in the biochemical industry.

Appendix I: The code metadata.

Code metadata description	Supplementary information
Current code version	v1.0
Permanent link to code/repository used for this code version	https://github.com/Tountain/SoundiationAcoustophoresis
Legal Code License	GNU GENERAL PUBLIC LICENSE V3.0
Code versioning system used	GitHub
Software code languages, tools, and services used	MATLAB
Compilation requirements, operating environments & dependencies	MATLAB 2010a and above
If available Link to developer documentation/manual	https://github.com/Tountain/SoundiationAcoustophoresis/tree/main/docs/user_manual

Appendix II: Scalar scattering coefficients for Cauchy boundary condition.

For the spherical objects, the scalar scattering coefficients for different boundary conditions are concluded in [40]. For non-spherical objects, we provide a method to evaluate the scalar scattering coefficients for the non-spherical objects with Cauchy boundary condition. The Cauchy boundary condition is the case in which the body consists of a fluid with material properties other than that of the surrounding fluid and does not support a shear wave. To derive the scalar scattering coefficients, the conformal transformation mapping is firstly needed to map the non-spherical object in physical space to a sphere in mapping space, i.e., (u, w, v) system [1][2].

On the mapping coordinate system, the compressible (Cauchy) boundary condition requires that the exterior and interior potential and particle velocity are equal on the surface of the scatterer $(u = u_0)$:

$$\rho_0\left[\hat{\phi}_{\text{ex}}(u_0, w, v) + \hat{\phi}_{\text{sc}}(u_0, w, v)\right] = \rho_{\text{p}}\hat{\phi}_{\text{int}}(u_0, w, v), \tag{B.1}$$

$$\vec{n} \cdot \nabla\left[\hat{\phi}_{\text{ex}}(u_0, w, v) + \hat{\phi}_{\text{sc}}(u_0, w, v)\right] = \vec{n} \cdot \nabla\left[\hat{\phi}_{\text{int}}(u_0, w, v)\right],$$

where $\hat{\phi}_{\text{ex}}(u_0, w, v)$, $\hat{\phi}_{\text{sc}}(u_0, w, v)$, and $\hat{\phi}_{\text{int}}(u_0, w, v)$ are the external, scattering, and transmitted velocity potential functions, respectively. ρ_{p} is the density of the particle. The external and scattering potential functions are given, respectively, in Eqs. (13) and (14) of [1], while the transmitted potential functions are:

$$\hat{\phi}_{\text{int}}(u_0, w, v) = \sum_{n,m} t_{nm} J_n^m\left(k_{\text{p}} u_0, w, v\right), \tag{B.2}$$

where t_{nm} is the transmission coefficients, and k_{p} is the wavenumber inside the particle. Then, the compressible boundary condition (or Eq. (B.1)) becomes

$$\rho_0\left[\sum_{n,m} \tilde{a}_{nm} J_n^m(ku_0, w, v) + \sum_{n,m} s_{nm}\tilde{a}_{nm} H_n^m(ku_0, w, v)\right] \tag{B.3}$$

$$= \rho_{\text{p}} \sum_{n,m} t_{nm} J_n^m\left(k_{\text{p}} u_0, w, v\right),$$

$$\vec{n}\cdot\nabla\left[\sum_{n,m}\tilde{a}_{nm}J_n^m(ku_0,w,v)+\sum_{n,m}s_{nm}\tilde{a}_{nm}H_n^m(ku_0,w,v)\right]$$
$$=\vec{n}\cdot\nabla\left[\sum_{n,m}t_{nm}J_n^m\left(k_{\mathrm{p}}u_0,w,v\right)\right].$$

Considering the relationship $\vec{n}\cdot\nabla(\cdot)=\frac{1}{\sqrt{f_u^2+f_w^2}}\frac{\partial(\cdot)}{\partial u}$ on the mapping coordinate system (seeing Eq. (B.11) of [2]), where the mapping function f is given in Eq. (9b), equation (B.3) becomes

$$\rho_0\left[\sum_{n,m}\tilde{a}_{nm}J_n^m(ku_0,w,v)+\sum_{n,m}s_{nm}\tilde{a}_{nm}H_n^m(ku_0,w,v)\right] \tag{B.4}$$
$$=\rho_{\mathrm{p}}\sum_{n,m}t_{nm}J_n^m\left(k_{\mathrm{p}}u_0,w,v\right),$$

$$\sum_{n,m}\tilde{a}_{nm}J_{n,u}^m(ku_0,w,v)+\sum_{n,m}s_{nm}\tilde{a}_{nm}H_{n,u}^m(ku_0,w,v)$$
$$=\sum_{n,m}t_{nm}J_{n,u}^m\left(k_{\mathrm{p}}u_0,w,v\right).$$

We multiply both sides of this equation by a set of spherical angular eigenfunctions $\psi_{n'}^{m'}(w,v)=P_{n'}^{m'}\left(\cos(w)\right)\sin(w)\mathrm{e}^{-m'v\mathrm{i}}$, and integrating over the range of w and v

$$\rho_0\int_0^{\pi}\int_0^{2\pi}\left[\sum_{n,m}\tilde{a}_{nm}J_n^m(ku_0,w,v)\right. \tag{B.5}$$
$$\left.+\sum_{n,m}s_{nm}\tilde{a}_{nm}H_n^m(ku_0,w,v)\right]\psi_{n'}^{m'}(w,v)\mathrm{d}v\mathrm{d}w$$
$$=\rho_{\mathrm{p}}\int_0^{\pi}\int_0^{2\pi}\left[\sum_{n,m}t_{nm}J_n^m\left(k_{\mathrm{p}}u_0,w,v\right)\right]\psi_{n'}^{m'}(w,v)\mathrm{d}v\mathrm{d}w,$$

$$\int_0^{\pi}\int_0^{2\pi}\left[\sum_{n,m}\tilde{a}_{nm}J_{n,u}^{m}(ku_0,w,v)\right.$$
$$\left.+\sum_{n,m}s_{nm}\tilde{a}_{nm}H_{n,u}^{m}(ku_0,w,v)\right]\psi_{n'}^{m'}(w,v)\mathrm{d}v\mathrm{d}w$$
$$=\int_0^{\pi}\int_0^{2\pi}\left[\sum_{n,m}t_{nm}J_{n,u}^{m}(k_{\mathrm{p}}u_0,w,v)\right]\psi_{n'}^{m'}(w,v)\mathrm{d}v\mathrm{d}w.$$

Considering the orthogonality relationship $\int_0^{2\pi}\mathrm{e}^{nw\mathrm{i}}\cdot\mathrm{e}^{-mw\mathrm{i}}\mathrm{d}w=2\pi\delta_{n,m}$ and the definition of spherical harmonic function $Y_n^m(\theta,\varphi)=\sqrt{\frac{(2n+1)}{4\pi}\cdot\frac{(n-m)!}{(n+m)!}}P_n^m\big(\cos(\theta)\big)\mathrm{e}^{m\varphi\mathrm{i}}$ [28], the above equation becomes

$$\rho_0\left[\sum_{n=0}^{N}\tilde{a}_{nm'}\Gamma_n^{n',m'}+\sum_{n=0}^{N}s_{nm'}\tilde{a}_{nm'}\Lambda_n^{n',m'}\right]=\rho_{\mathrm{p}}\left[\sum_{n=0}^{N}t_{nm'}\bar{\Gamma}_n^{n',m'}\right],\tag{B.6}$$
$$\sum_{n=0}^{N}\tilde{a}_{nm'}\Gamma_{n,u}^{n',m'}+\sum_{n=0}^{N}s_{nm'}\tilde{a}_{nm'}\Lambda_{n,u}^{n',m'}=\sum_{n=0}^{N}t_{nm'}\bar{\Gamma}_{n,u}^{n',m'},$$
$$(n'=0,1,\cdots,N;m'=-N,\cdots,0,\cdots,N)$$

where the structural functions $\Gamma_n^{n',m'}$ and $\Lambda_n^{n',m'}$, and their partial derivatives $\Gamma_{n,u}^{n',m'}$ and $\Lambda_{n,u}^{n',m'}$, are given in Eq. (8). The structural function $\bar{\Gamma}_n^{n',m'}$ and its partial derivatives $\bar{\Gamma}_{n,u}^{n',m'}$ follow the same formulas given in Eq. (8), while the wavenumber changes to the wavenumber of the particle k_{p}. It can be found that for each combination of (n',m'), we can obtain an additional equation to close the system. The upper matrix and lower matrix, respectively, provide $(N+1)\times(2N+1)$ additional equations, and therefore totally $2\times(N+1)\times(2N+1)$ additional equations. There are $(N+1)\times(2N+1)$ unknown scalar scattering coefficients $s_{n'm'}$ and $(N+1)\times(2N+1)$ unknown transmission coefficients $t_{n'm'}$. Hence, $s_{n'm'}$ and $t_{n'm'}$ can be solved using Eq. (B.6), and the solved scalar scattering coefficients $s_{n'm'}$ can be directly inserted into Eqs. (10) and (11) for the radiation force and torque on the compressible objects (following the Cauchy boundary condition).

References

[1]. T. Tang, and L. Huang, “An efficient semi-analytical procedure to calculate acoustic radiation force and torque for axisymmetric irregular bodies,” Journal of Sound and Vibration **532**, 117012 (2022).

[2]. T. Tang, and L. Huang, “Theoretical framework to predict the acoustophoresis of axisymmetric irregular objects above an ultrasound transducer array,” Physical Review E **105**, 055110 (2022).

[3]. P. J. Westervelt, “The theory of steady forces caused by sound waves,” The Journal of the Acoustical Society of America **23**(3), 312–315 (1951).

[4]. P. J. Westervelt, “Acoustic radiation pressure,” The Journal of the Acoustical Society of America **29**(1), 26–29 (1957).

[5]. G. Maidanik, “Torques due to acoustical radiation pressure,” The Journal of the Acoustical Society of America **30**(7), 620–623 (1958).

[6]. L. Zhang, and P. L. Marston, “Angular momentum flux of nonparaxial acoustic vortex beams and torques on axisymmetric objects,” Physical Review E **84**(6), 065601 (2011).

[7]. G. T. Silva, “Acoustic radiation force and torque on an absorbing compressible particle in an inviscid fluid,” The Journal of the Acoustical Society of America **136**(5), 2405–2413 (2014).

[8]. J. P. Leão-Neto, and G. T. Silva, “Acoustic radiation force and torque exerted on a small viscoelastic particle in an ideal fluid,” Ultrasonics **71**, 1–11 (2016).

[9]. L. Zhang, and P. L. Marston, “Acoustic radiation torque and the conservation of angular momentum (L),” The Journal of the Acoustical Society of America **129**(4), 1679–1680 (2011).

[10]. A. Marzo, and B. W. Drinkwater, “Holographic acoustic tweezers,” Proceedings of the National Academy of Sciences **116**(1), 84–89 (2019).

[11]. R. Hirayama, D. M. Plasencia, N. Masuda, and S. Subramanian, “A volumetric display for visual, tactile and audio presentation using acoustic trapping,” Nature **575**(7782), 320–323 (2019).

[12]. M. Baudoin, J. L. Thomas, R. A. Sahely, J. C. Gerbedoen, Z. Gong, A. Sivery, O. B. Matar, N. Smagin, P. Favreau, and A. Vlandas, “Spatially selective manipulation of cells with single-beam acoustical tweezers,” Nature Communications **11**, 4244 (2020).

[13]. D. Baresch, and V. Garbin, “Acoustic trapping of microbubbles in complex environments and controlled payload release,” Proceedings of the National Academy of Sciences **117**(27), 15490–15496 (2020).

[14]. C. Chen, Y. Gu, J. Philippe, P. Zhang, H. Bachman, J. Zhang, J. Mai, J. Rufo, J. F. Rawls, E. E. Davis, and T. J. Huang, “Acoustofluidic rotational tweezing enables high-speed contactless morphological phenotyping of zebrafish larvae,” Nature Communications **12**, 1118 (2021).

[15]. B. Neumann, K. C. Nguyen, D. H. Hall, A. Ben-Yakar, and M. A. Hilliard, “Axonal regeneration proceeds through specific axonal fusion in transected C. elegans neurons,” Developmental Dynamics **240**(6), 1365–1372 (2011).

[16]. L. P. Gor’kov, “Forces acting on a small particle in an acoustic field within an ideal fluid,” Doklady Akademii Nauk **140**, 88–91 (1961).

[17]. Z. Gong, and M. Baudoin, “Equivalence between angular spectrum-based and multipole expansion-based formulas of the acoustic radiation force and torque,” The Journal of the Acoustical Society of America **149**(5), 3469–3482 (2021).

[18]. L. Zhang, and P. L. Marston, “Geometrical interpretation of negative radiation forces of acoustical Bessel beams on spheres,” Physical Review E **84**(3), 035601 (2011).

[19]. G. T. Silva, “An expression for the radiation force exerted by an acoustic beam with arbitrary wavefront (l),” The Journal of the Acoustical Society of America 130(6), 3541–3544 (2011).

[20]. G. T. Silva, T. Lobo, and F. Mitri, “Radiation torque produced by an arbitrary acoustic wave,” EPL (Europhysics Letters) **97**(5), 54003 (2012).

[21]. P. Hahn, I. Leibacher, T. Baasch, and J. Dual, “Numerical simulation of acoustofluidic manipulation by radiation forces and acoustic streaming for complex particles,” Lab on a Chip **15**(22), 4302–4313 (2015).

[22]. Z. Gong, W. Li, F. G. Mitri, Y. Chai, and Y. Zhao, “Arbitrary scattering of an acoustical Bessel beam by a rigid spheroid with large aspect-ratio,” Journal of Sound and Vibration **383**, 233–247 (2016).

[23]. Z. Gong, and M. Baudoin, “Acoustic radiation torque on a particle in a fluid: An angular spectrum based compact expression,” The Journal of the Acoustical Society of America **148**, 3131–3140 (2020).

[24]. D. Ahmed, A. Ozcelik, N. Bojanala, N. Nama, A. Upadhyay, Y. Chen, W. Hanna-Rose, and T. J. Huang, “Rotational manipulation of single cells and organisms using acoustic waves,” Nature Communications **7**, 11085 (2016).

[25]. P. Glynne-Jones, P. P. Mishra, R. J. Boltryk, and M. Hill, “Efficient finite element modeling of radiation forces on elastic particles of arbitrary size and geometry,” The Journal of the Acoustical Society of America **133**(4), 1885–1893 (2013).

[26]. T. Tang, and L. Huang, “Acoustic radiation force for multiple particles over a wide size-scale by multiple ultrasound sources,” Journal of Sound and Vibration **532**, 116256 (2021).

[27]. J. Fankhauser, C. Goering, and J. Dual, “OSAFT Library: An Open-Source Python Library for Acoustofluidics,” Frontiers in Physics 445 (2022).

[28]. E. G. Williams, *Fourier acoustics: sound radiation and nearfield acoustical holography*, Academic Press (1999).

[29]. P. A. Martin, *Multiple scattering: interaction of time-harmonic waves with N obstacles*, Cambridge University Press (2006).

[30]. D. T. DiPerna, and T. K. Stanton, “Sound scattering by cylinders of noncircular cross-section: A conformal mapping approach,” The Journal of the Acoustical Society of America **96**(5), 3064–3079 (1994).

[31]. G. T. Silva, “Off-axis scattering of an ultrasound Bessel beam by a sphere,” IEEE Transactions on Ultrasonics, Ferroelectrics, and Frequency Control **58**(2), 298–304 (2011).

[32]. P. L. Marston, and J. H. Crichton, “Radiation torque on a sphere caused by a circularly-polarized electromagnetic wave,” Physical Review A **30**(5), 2508 (1984).

[33]. G. G. Stokes, “On the effect of the internal friction of fluids on the motion of pendulums,” Trans. Camb. Phil. Soc. **9**(8), (1851).

[34]. G. Kirchhoff, and K. Hensel, *Vorlesungen über mathematische Physik: Mechanik*, B. G. Teubner (1883).

[35]. J. D. N. Cheeke, *Fundamentals and applications of ultrasonic waves*, CRC Press (2017).

[36]. B. W. Drinkwater, “Dynamic-field devices for the ultrasonic manipulation of microparticles,” Lab on a Chip **16**(13), 2360–2375 (2016).

[37]. T. Tang, B. Dong, and L. Huang, “Agglomeration of particles by a converging ultrasound field and their quantitative assessments,” Ultrasonics Sonochemistry **75** 105590 (2021).

[38]. A. D. Maxwell, M. Bailey, B. W. Cunitz, M. Terzi, A. Nikolaeva, S. Tsysar, and O. A. Sapozhnikov, “Vortex beams and radiation torque for kidney stone management,” The Journal of the Acoustical Society of America **139**(4), 2040–2040 (2016).

[39]. M. A. Ghanem, A. D. Maxwell, Y.-N. Wang, B. W. Cunitz, V. A. Khokhlova, O. A. Sapozhnikov, and M. R. Bailey, “Noninvasive acoustic manipulation of objects in a living body,” Proceedings of the National Academy of Sciences **117**(29), 16848–16855 (2020).

[40]. Z. Gong, and M. Baudoin, “Single beam acoustical tweezers based on focused beams: A numerical analysis of 2D and 3D trapping capabilities,” ArXiv: 2205.10033 (2022).